Growth and Optoelectronic Properties of III-Nitride Quaternary Alloys

J. Li, K. B. Nam, K. H. Kim, T. N. Oder, H. J. Jun, J. Y. Lin, and H. X. Jiang[a)]

Department of Physics, Kansas State University, Manhattan, KS 66506-2601

ABSTRACT

$In_xAl_yGa_{1-x}N$ quaternary alloys with different In and Al compositions were grown on sapphire substrates with GaN buffer by metal-organic chemical vapor deposition (MOCVD). Optical properties of these quaternary alloys were studied by picosecond time-resolved photoluminescence. Our studies have revealed that $In_xAl_yGa_{1-x}N$ quaternary alloys with lattice matched with GaN (y~4.7x) have the highest optical quality. More importantly, we can achieve not only higher emission energies but also higher emission intensities (or quantum efficiencies) in $In_xAl_yGa_{1-x-y}N$ quaternary alloys than that of GaN. The quantum efficiency of $In_xAl_yGa_{1-x}N$ quaternary alloys was also enhanced significantly over AlGaN alloys with a comparable Al content. We have also fabricated ultraviolet (UV) photoconductive detectors based on $In_xAl_yGa_{1-x-y}N$/GaN quaternary alloy heterostructures. We found that with varying In and Al compositions, the cut-off wavelength of the $In_xAl_yGa_{1-x-y}N$ detectors could be varied to the deep UV range and that the responsivity of the $In_xAl_yGa_{1-x-y}N$ quaternary alloys exceeded that of AlGaN alloys with comparable cut-off wavelengths by a factor of five. This showed that $In_xAl_yGa_{1-x-y}N$ quaternary alloys is a very important material for solar-blind UV detector applications particularly in the deep UV range where Al rich AlGaN alloys have problems with low quantum efficiency and cracks due in part to lattice mismatch with GaN. Our results strongly suggested that $In_xAl_yGa_{1-x-y}N$ quaternary alloys open a new avenue for the fabrication of many novel optoelectronic devices such as high efficient light emitters and detectors, particularly in the UV region.

Keywords: GaN, InAlGaN quaternary alloys, AlGaN alloys, wide bandgap, time-resolved PL, optical transitions, UV detectors

1. INTRODUCTION

III-nitrides including GaN epilayers, InGaN and AlGaN alloys, and InGaN/GaN and GaN/AlGaN multiple quantum wells (MQWs) have been intensively studied due to their many applications in UV/blue light emitters, solar-blind UV detectors, and high power/temperature electronics[1]. It has been demonstrated that most nitride based devices must take advantage of MQWs and heterostructures such as GaN/AlGaN and InGaN/GaN as well as the tunability of the band gaps in the alloys from InN (1.9 eV) to GaN (3.4 eV) and to AlN (6.2 eV). Thus an important issue is still QW or heterostructure device structural perfection, which requires development of innovative approaches to synthesize high quality III-nitride QWs and heterostructures. As illustrated in Fig. 1 that the photoluminescence (PL) emission intensity or quantum efficiency and the electron mobility of $Al_xGa_{1-x}N$ alloys decrease exponentially with an increase of Al-content.[2] The quantum efficiencies of UV light emitters fabricated from $Al_xGa_{1-x}N$ alloys are thus expected to drop significantly as the emission energy extends into deeper UV region. This is one of the key problems for the fabrication of high performance UV optoelectronic devices. In fact, in a recent proof-of-concept demonstration work, an output power of 13 μW at 20 mA was measured from an AlGaN/GaN MQW light emitting diode (LED) in the UV spectral region near 354 nm.[3] This output power is more than two orders of magnitude lower than a 3 mW output power from blue LEDs fabricated from InGaN/GaN MQWs. GaN-based photodetectors showing high gain have also been reported. These included photoconductors [4], p-n junction detectors [5] and metal-semiconductor-metal detectors [6]. To take advantage of the tunability of the cut-off wavelengths, AlGaN-based photoconductors [7], visible-blind UV cameras based on GaN/AlGaN p-i-n photodiode arrays [8] and Schottky diode detectors [9] and have been fabricated. Further applications of AlGaN are feasible with an increased Al content. However, a major drawback in the use of AlGaN alloys come from the lattice mismatch with GaN in the AlGaN/GaN heterostructure, in particular at high Al content. The result of this is local strain relaxation at the heterointerface through generation of cracks and/or misfit dislocations.

A material that is both lattice-matched with GaN and whose band-gap energy can be adjusted for UV applications is therefore desirable. Such a material would be more versatile and would replace AlGaN, which is the current choice for
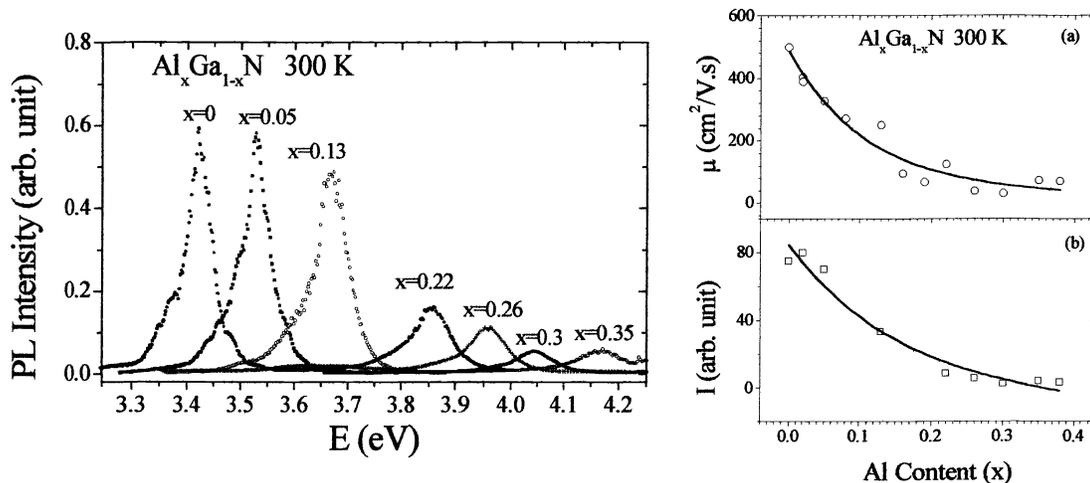
Figure 1. (Left) PL Spectra of $Al_xGa_{1-x}N$ measured at 300 K. (Right) Electron mobility and integrated PL emission intensity vs Al content measured at 300 K. The results show that both the emission intensity and the electron mobility of $Al_xGa_{1-x}N$ decrease exponentially with x - a potential problem for $Al_xGa_{1-x}N$ as active media for UV optoelectronic devices.

nitride UV emitters and detectors. Recently, $In_xAl_yGa_{1-x-y}N$ quaternary alloys have been recognized to have the potential to overcome some shortfall of GaN epilayers and InGaN and AlGaN alloys[10-16]. By varying In and Al compositions x and y in $In_xAl_yGa_{1-x-y}N$, one can change the energy band gap while keep lattice matched with GaN. In addition to the key features of lattice-match with GaN and the tunability in energy bandgap, $In_xAl_yGa_{1-x-y}N$ quaternary alloys also have the potential to provide a better thermal match to GaN, which could be an important advantage in epitaxial growth. For lattice matching with GaN, the ratio of the concentration of In: Al can be estimated from the formula:

$$a[In_xAl_yGa_{1-x-y}N] = xa_{InN} + ya_{AlN} + (1-x-y)a_{GaN}. \qquad (1)$$

This assumes that a solid solution of InN, AlN and GaN are present in the quaternary [11-13]. Using values of the lattice constant a_{InN} = 3.548 Å, a_{AlN} = 3.112 Å, and a_{GaN} = 3.189 Å, the ratio x:y of the concentration of In:Al is found to be around 1:4.7 for lattice matching with GaN. When this ratio is inserted in the formula for energy gap (E_g), one obtains the following energy gap variation of $In_xAl_yGa_{1-x-y}N$:

$$E_g[In_xAl_{4.7x}Ga_{1-5.7x}N] = xE_g(InN) + 4.7xE_g(AlN) + (1-5.7x)E_g(GaN) \qquad (2)$$
$$= (3.4 + 11.5x) \; eV \; = \; [3.4, 5.5] \; eV$$

with 0 < x < 0.18 and where we have used $E_g(InN)$ = 1.9 eV, $E_g(AlN)$ = 6.2 eV and $E_g(GaN)$ = 3.4 eV. The bowing effects are not included in Eq. (2) since no data is available for the energy gap of InAlGaN quaternary alloys. This indicates the possibility of growing $In_xAl_yGa_{1-x-y}N$ lattice-matched to GaN with band gap energy adjustable from 3.4 to 5.5 eV for deep UV optoelectronic applications. In this paper, we report the growth and picosecond time-resolved photoluminescence studies of ternary (InGaN and AlGaN) and $In_xAl_yGa_{1-x-y}N$ quaternary alloys and the fabrication and characterization of UV photoconductive detectors based on these materials.

2. EXPERIMENTAL

A semi-insulating 0.5-1.0 μm GaN epilayer was first deposited on the sapphire substrate with a 25 nm low temperature GaN buffer layer, followed by the deposition of a 0.1 μm $In_xAl_yGa_{1-x-y}N$ quaternary alloy epilayer by metal-organic chemical vapor deposition (MOCVD). A few InAlGaN quaternary alloys were also grown directly on top of the GaN buffer layer for the purpose of comparison. Additionally, GaN epilayers, and InGaN and AlGaN ternary alloys were also grown on the sapphire substrates for comparison studies. The sources used were trimethylgallium (TMG), trimethylaluminum (TMAl), trimethylindium (TMIn) and ammonia. The growth temperature and pressure for the underneath GaN epilayer were 1050 °C and 300 Torr, respectively. Different In concentrations in the quaternary alloys were achieved by varying the flow rate (30-100 sccm) of the indium source or

by changing the growth temperature (780-820°C) for a given flow rate of the In source. Hall measurements showed that the mobility of the quaternary samples grown over GaN epilayers, depending on In and Al contents, was 235 - 500 cm^2/V-sec with electron concentration of 2.3 – 6.0 x 10^{17} cm^{-3} while the mobility of those grown directly on GaN buffer layers varied from 34 - 45 cm^2/V-sec. Atomic force microscopy (AFM) was employed to study the surface morphologies and no cracking at the surface of the quaternary samples were noticed [Fig. 2 (a)]. This is an indication of possibly better lattice as well as thermal matching of quaternary alloys with GaN than AlGaN alloys. Picosecond time-resolved PL was employed to study the optical properties of these materials[17]. The excitation laser wavelength and average pumping power were 290 nm and 20 mW, respectively. The time-resolved PL signals were dispersed by a 1.3 m monochrometer and collected by a streak camera (Hamamatsu C5680). Contents of In and Al were determined by different methods including X-ray diffraction (XRD), energy dispersal system (EDS), Rutherford back scattering (RBS), and photoluminescence (PL) measurements and were within 5% variation. RBS measurements have shown that the In and Al contents in the quaternary In$_x$Al$_y$Ga$_{1-x-y}$N sample #706 were x=0.026 and y=0.124 respectively. Hence the ratio of the concentration of In:Al in sample # 706 was about 1:4.7 which is close to the estimated value of 1:4.7 needed for lattice matching with GaN.

To fabricate the photoconductive UV detector, samples were cut into 3 mm x 3 mm pieces and cleaned with organic solvents followed by a 20 second dip in buffered hydrofluoric acid to etch off surface oxides. A pair of multilayered ohmic contacts of Ti/Al/Ni/Au with thickness of 15/220/40/50 nm respectively was deposited on each sample in an electron beam evaporating system with a base pressure of about 5 x 10^{-7} torr. A gap of width 1 mm was defined between the contacts with a shadow mask used during the e-beam deposition. The current-voltage measurement across the contacts indicated linear characteristics even without annealing. In the measurement of the photoconductance, we used a 150-watt halogen lamp together with a 0.3 m monochromator as the excitation source. The monochromator had a grating of 1200 grooves/mm with peak sensitivity at 300 nm. Collimating lenses and a short pass filter were used. Our set-up employed a Wheatstone bridge circuit to improve the sensitivity of the measurement. The sample was connected as one of the arms of the circuit. Prior to the measurements, the samples were kept in the dark and the dark current balanced to zero across the electrometer used. When the light was turned on, the wavelength of the incident light was step-scanned slowly from long to short wavelength to minimize possible effects of persistent photoconductivity. The current I$_{ph}$ detected by the electrometer as a function of the wavelength of the incident light was recorded. The incident light intensity was normalized using a Hamamatsu photomultiplier tube.

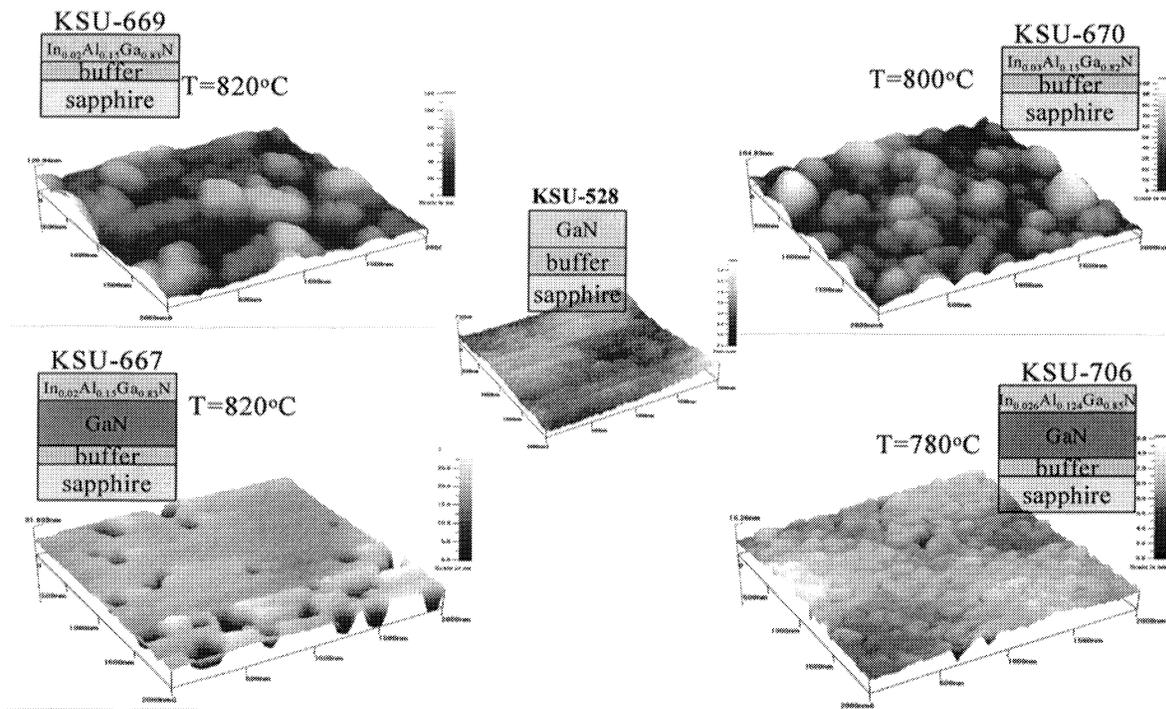## InAlGaN Quaternary Alloys (2μm x 2μm AFM image)

Figure 2(a) Atomic force microscopy (AFM) images (2 μm x 2 μm scan) for four InAlGaN quaternary samples of varying structures and a GaN epilayer.
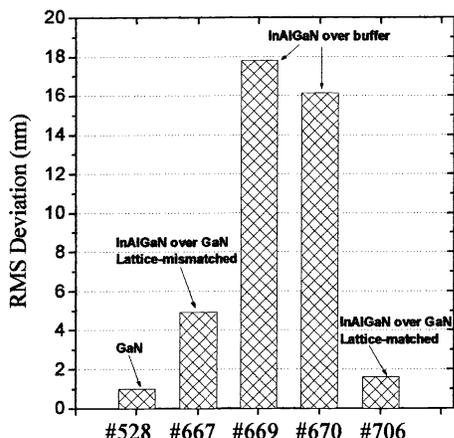
3. RESULTS AND DISCUSSIONS

Figure 2(b). Atomic force microscopy (AFM) values of root-mean-square (rms) deviations of surface morphology of InAlGaN alloys. Sample #706 ($In_{0.026}Al_{0.124}Ga_{0.85}N$) grown over GaN and lattice-matched with GaN has a smallest rms value comparable to that of GaN.
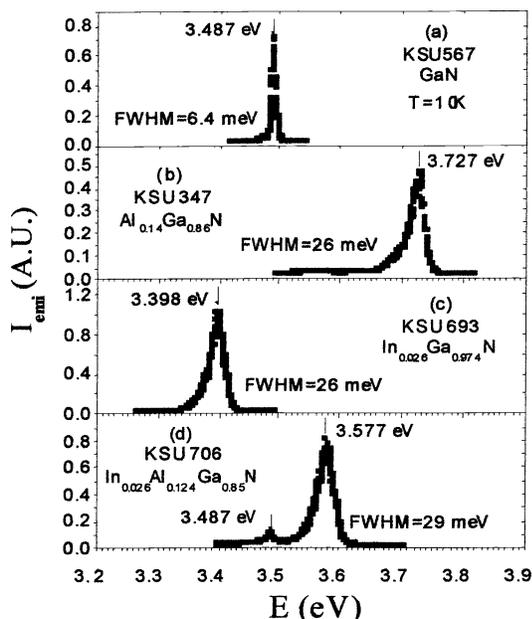

Figure 3. PL spectra of GaN, AlGaN, InGaN, and InAlGaN measured at 10 K. We can achieve not only higher emission energies but also higher emission efficiencies in the UV region in InAlGaN quaternaries than that in GaN. The emission efficiency of the InAlGaN epilayers is also higher than that of the AlGaN epilayer and is comparable to that of the InGaN epilayer.

Figure 2(a) shows atomic force microscopy (AFM) images (2 μm x 2 μm scan) for four InAlGaN quaternary samples of varying structures and a GaN epilayer. The results of Fig. 2(a) is summarized in Fig. 2(b), where the AFM values of root-mean-square (rms) deviations of surface morphology are shown for InAlGaN alloys. It can be seen that sample #706 ($In_{0.026}Al_{0.124}Ga_{0.85}N$) grown over GaN and lattice-matched with GaN has smallest rms value comparable to that of GaN. Sample #667 ($In_{0.02}Al_{0.15}Ga_{0.83}N$) also grown over GaN but lattice-mismatched to GaN has poorer surface morphology with rms deviation three times higher than #706. On the other hand, InAlGaN quaternary layers grown directly over GaN buffer (#669 & 670) show much larger AFM rms deviations. Thus a good lattice match of the quaternary InAlGaN with GaN results in a smoother surface morphology.

Time–resolved PL has been employed to study the mechanisms of the optical transitions as well as to characterize the quality of the grown epilayers. It was found that $In_xAl_yGa_{1-x-y}N$ quaternary alloys with lattice matched with GaN epilayers (y~4.7x) have the highest PL emission intensity as well as the narrowest XRD linewidth. Table 1 lists the optimal growth parameters and emission properties of one of the $In_xAl_yGa_{1-x-y}N$ quaternary alloys that is lattice matched with GaN (sample #706) together with those of $In_xGa_{1-x}N$ and $Al_xGa_{1-x}N$ alloys. Room temperature electron mobilities and concentrations have also been measured and listed in Table 1 as well.

Figure 3 shows the PL emission spectra of GaN epilayer, $Al_xGa_{1-x}N$ alloy (#607), $In_xGa_{1-x}N$ alloy (#693), and $In_xAl_yGa_{1-x-y}N$ quaternary alloy (#706) measured at T=10 K. The arrows indicate the spectral peak positions. The full width at half maximum (FWHM) of each emission line is also included in the figure. The integrated PL intensity, I_{emi}, for each of the alloy samples is included in Table 1. The lower emission peak at 3.487 eV in the PL spectrum of InAlGaN quaternary alloy in Fig. 3(d) is due to the underneath GaN epilayer. The emission spectrum of $In_xAl_yGa_{1-x-y}N$ quaternary alloys in Fig. 3(d) shows that we can achieve not only higher emission energies but also higher emission efficiency in $In_xAl_yGa_{1-x-y}N$ quaternary alloys than that of GaN. The emission intensity of $In_xAl_yGa_{1-x-y}N$ quaternary alloys is also higher than that of $Al_xGa_{1-x}N$ alloy by a factor of 2.2 and 3.6 at 10 and 300 K, respectively and is comparable to that of $In_xGa_{1-x}N$ alloy. The physical origin of this enhanced quantum efficiency (QE) in $In_xAl_yGa_{1-x-y}N$ quaternary alloys over GaN and $Al_xGa_{1-x}N$ alloy is not yet clear. However, it is now well known that low In-content $In_xGa_{1-x}N$ alloys have higher quantum efficiencies than GaN epilayers. It is thus not surprising that the QE is enhanced after the incorporation of indium into $Al_xGa_{1-x}N$.

Table 1. Comparison of InAlGaN Quaternary Alloys with InGaN and AlGaN

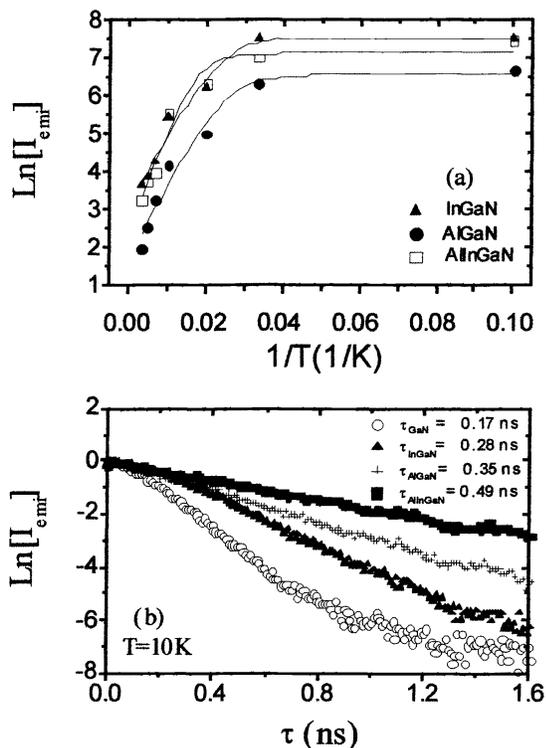| Samples	$In_xGa_{1-x}N$	$Al_xGa_{1-x}N$	$In_xAl_yGa_{1-x-y}N$
Growth Parameters			
P (Torr)	300	270	300
T (°C)	780	1060	780
XRD (002) (arcsec)	359	375	411
In and Al Contents	x~0.026	x~0.136	x~0.026, y~0.124
μ (cm^2/Vs)	222	215	236
n (10^{17} cm^{-3})	2.50	5.40	3.60
E_p (eV) T=10 K	3.395	3.722	3.575
T=300 K	3.348	3.674	3.542
I_{emi} (A.U.) T=10K	185	80	175
T=300K	3.9	0.72	2.58
FWHM (meV)	26	26	29
$E_{activation}$ (meV)	16.3	16.7	23.4
τ (ns) (T=10K)	0.28	0.35	0.49

Figure 4 (a) The Arrhenius plots of PL emission intensities of InAlGaN, InGaN, and AlGaN alloys. (b) PL decay profile of InAlGaN quaternary alloy together with those of GaN epilayers, InGaN, and AlGaN alloys measured at T=10 K.
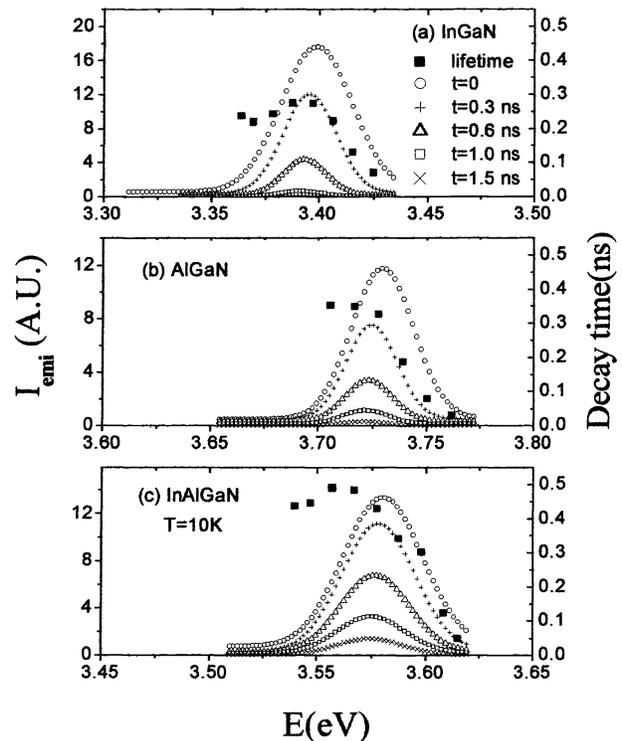
Figure 5. Time-resolved PL spectra as well as emission energy dependence of decay lifetime measured at 10 K for (a) $In_xGa_{1-x}N$ alloys, (b) $Al_xGa_{1-x}N$ alloys, and (c) $In_xAl_yGa_{1-x-y}N$ quaternary alloys.

From Table 1, it is interesting to note that the growth conditions as well as the emission properties of $In_xAl_yGa_{1-x-y}N$ quaternary alloys are more closely related with $In_xGa_{1-x}N$ than $Al_xGa_{1-x}N$. The growth temperature and pressure for the optimized $In_xAl_yGa_{1-x-y}N$ quaternary alloys (T=780 ^{0}C and P=300 τ) are exactly the same as for $In_xGa_{1-x}N$ alloys. The relative integrated PL emission intensities of $In_xAl_yGa_{1-x-y}N$ quaternary alloys are 175 (T=10 K) and 2.58 (T=300 K). These values are comparable with the values of 185 (T=10 K) and 3.9 (T= 300 K) for InGaN, but much higher than the values of 80 (T=10 K) and 0.72 (T=300K) for AlGaN. It is thus concluded that $In_xAl_yGa_{1-x-y}N$ quaternary alloys are InGaN-like rather than AlGaN-like, although Al composition is almost a factor of 5 larger than In.

PL emission spectra at different temperatures were also measured for InAlGaN, InGaN and AlGaN alloys. Emission intensities in these samples all decrease with increasing temperature. The Arrhenius plots of PL emission intensity of InAlGaN, InGaN and AlGaN alloys are shown in Fig. 4(a). The solid lines in Fig. 4(a) are the least squares fit of data with equation

$$I(T)=I_0/[1+Cexp(-E_0/kT)], \tag{3}$$

where E_0 is the activation energy and C is a fitting constant. The fitted values of E_0 are 16.3, 16.7, and 23.4 meV for InGaN, AlGaN, and InAlGaN alloys, respectively.

The dominant PL transitions in $In_xAl_yGa_{1-x-y}N$ quaternary alloys at low temperatures are due to the localized exciton recombination, just as the cases in InGaN and AlGaN alloys. This fact is reflected in the characteristics of time-resolved PL as well as decay lifetimes. Decay lifetimes of PL emission at their spectral peak positions were also measured for InAlGaN, InGaN and AlGaN alloys and Fig. 4(b) shows the PL decay profiles measured at their corresponding spectral peak positions at 10 K. The measured decay lifetimes at 10 K for InGaN, AlGaN, and InAlGaN alloys are listed in Table 1.

In Fig. 5 is the plot of time-resolved PL spectra as well as the emission energy dependence of the decay lifetime measured at T=10 K for (a) $In_xGa_{1-x}N$ alloys, (b) $Al_xGa_{1-x}N$ alloys, and (c) $In_xAl_yGa_{1-x-y}N$ quaternary alloys. The behavior of emission energy dependence of decay lifetime is very similar among these three alloys. While InAlGaN has the longest decay lifetimes, the decay lifetime decreases with an increase of emission energy at energies above their corresponding spectral peak positions. This is a well-known character of localized excitons and is due to the transfer of excitons from higher to lower energy sites within the tail states caused by alloy fluctuations.[2,18]

The increased decay lifetime as well as activation energy in quaternary alloys points to an enhanced localization effects in $In_xAl_yGa_{1-x-y}N$ quaternary alloys compared with InGaN and AlGaN ternary alloys. The measured PL decay lifetime for $In_xAl_yGa_{1-x-y}N$ quaternary alloys at T=10 K, indicated in Table 1, is 0.49 ns, while that for InGaN and AlGaN are 0.28 and 0.35 ns, respectively. It is interesting that the measured decay lifetime of $In_xAl_yGa_{1-x-y}N$ quaternary alloys at T=10 K, $\tau_{InAlGaN}$, is correlated with those of InGaN and AlGaN alloys, τ_{InGaN} and τ_{AlGaN}, through with the relation $\tau_{InAlGaN}$=0.49 ns$\approx(\tau^2_{InGaN}+\tau^2_{AlGaN})^{1/2}=(0.28^2+0.35^2)^{1/2}$ =0.45 ns. This fact provides some hint that localization effects in $In_xAl_yGa_{1-x-y}N$ quaternary alloys are the summation of those in AlGaN and InGaN alloys with comparable In and Al compositions. Further evidence to support this speculation is that the relationship between the activation energies, E_0, in $In_xAl_yGa_{1-x-y}N$ quaternary alloys and InGaN and AlGaN ternary alloys as shown in Table 1 is the same as the decay lifetimes, i.e., $E_{0,InAlGaN}$=23.4 meV$\approx(E^2_{0,AlGaN}+E^2_{0,InGaN})^{1/2}$ =$(16.3^2+16.7^2)^{1/2}$ meV =23.3 meV.

Figure 6 shows the normalized photoresponse versus the excitation light wavelength for the $In_xAl_yGa_{1-x-y}N$ detectors with different In and Al contents. The photoresponse from two of the quaternary samples (#706 and #667) shown in figure 6 has a step at around 363 nm and this comes from the underlying GaN epilayer in those samples. The other two samples (#669 and #670) show no such step as they were grown directly on the thin buffer layer. The cut-off wavelengths of these two samples are not as sharp; perhaps due to the poor crystalline quality as also noted in the low values of their mobilities and higher AFM rms deviations of the surface morphology [shown in Figure 2(b)]. Our results reveal that the cut-off wavelength can be varied and in this case, from 345 to 289.6 nm, though the ratio of In:Al will no longer be constant at the value 1:4.7 required for exact lattice matching. The mismatch can be kept small enough to avoid cracking at the epilayer and yet achieve a significant change in the cut-off wavelength. Shown in this figure is also a decrease in photocurrent at shorter wavelengths. This is caused by surface recombination because at higher energies, absorption takes place closer to the surface [19,20].

Figure 7 shows the plot of the normalized photoresponse versus wavelength for a quaternary sample # 667 with approximate composition $In_{0.02}Al_{0.15}Ga_{0.83}N$ and an $Al_{0.14}Ga_{0.86}N$ sample #607 both with about the same cut-off wavelength (326.8 nm). It is noted that the response of the $In_{0.02}Al_{0.15}Ga_{0.83}N$ quaternary alloy was about five times greater than that of $Al_{0.14}Ga_{0.86}N$ of comparable cut-off wavelength. In order to suitably compare the photoresponse from two different alloys, it is important to choose those whose cut-off wavelengths are equal. This is important because photoresponse is found to
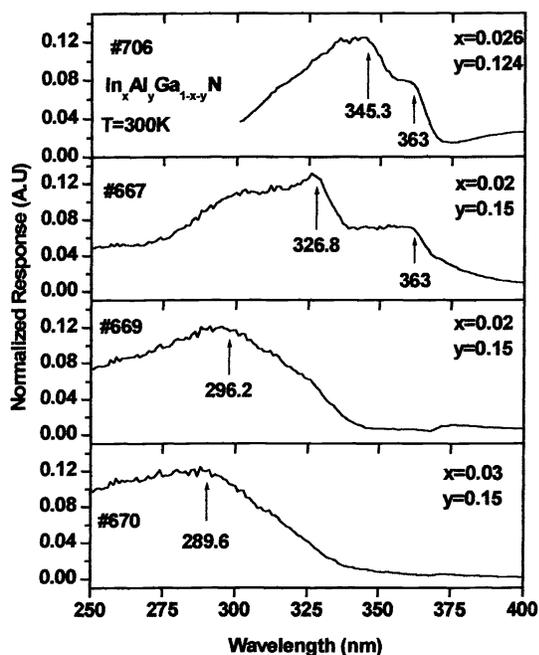
Figure 6. Normalized photoresponse versus wavelength of incident light of $In_xAl_yGa_{1-x-y}N$ quaternary alloys with different In and Al contents. The arrows indicate the cut-off wavelength for the quaternary alloys. The photoresponse from the underlying GaN epilayer in the two samples #706 and #667 is seen in the steps at 363 nm.
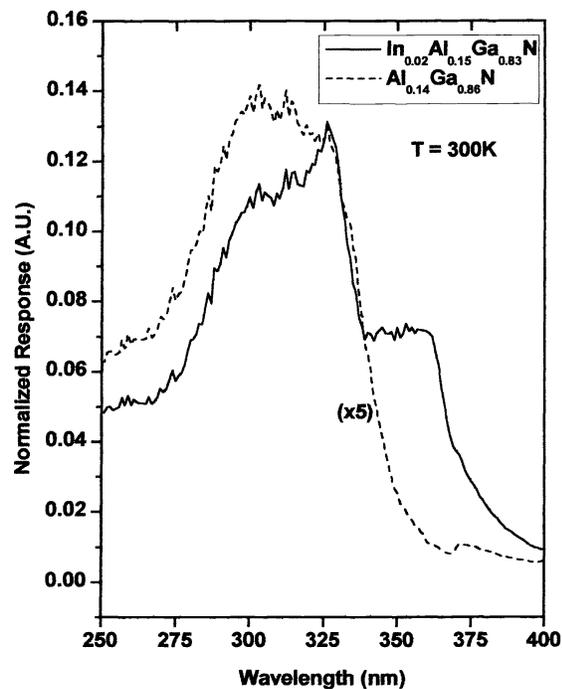
Figure 7. The response of $In_xAl_yGa_{1-x-y}N$ quaternary alloy (solid line) and $Al_yGa_{1-y}N$ alloy (dotted line) with comparable cut-off wavelength. The compositions for these samples are estimated to be $In_{0.02}Al_{0.15}Ga_{0.83}N$ and $Al_{0.14}Ga_{0.86}N$, respectively.

decrease with decreasing values of the cut-off wavelength.

We thus point at several potential advantages of $In_xAl_yGa_{1-x-y}N$ quaternary over $Al_yGa_{1-x-y}N$ ternary alloys. First is that $In_xAl_yGa_{1-x-y}N$ provides a photoconductive UV detector with photoresponse much larger than $Al_yGa_{1-x-y}N$ of comparable cut-off wavelength. This is particularly important, as the ternary alloy has been the one mostly used for UV detector applications. The reason for the enhancement of the photoresponse in $In_xAl_yGa_{1-x-y}N$ as compared with $Al_yGa_{1-x-y}N$ is not yet clearly understood. We speculate that this is perhaps related to enhanced quantum efficiency and/or improved heterointerface and the reduction of strain when In is incorporated into the AlGaN. The second advantage of $In_xAl_yGa_{1-x-y}N$ quaternary alloys is that they provide much higher emission intensities than those of AlGaN with a comparable Al composition. The possible physics involved here is probably very similar with that between GaN and InGaN. It has been now well established that emission intensity in low In-content InGaN alloys is much higher than that of GaN epilayers probably due to localization effects. It is thus not surprising that emission intensity of InAlGaN is higher than that of AlGaN, attributed probably again to the inherent properties associated with the presence of In. The enhanced emission intensity or QE have been observed recently in unstrained InGaN/InAlGaN QWs in which the quaternary serves as the barrier material and was attributed to the reduction of dislocation density as well as of the piezoelectric field.[13] Our results show that besides the advantages of reducing dislocation density and/or piezoelectric field in lattice-matched InGaN/InAlGaN and GaN/InAlGaN QWs, emission intensity or QE of InAlGaN is also higher than that of AlGaN with a comparable Al composition. This makes the InAlGaN quaternary alloys a better choice as active materials for many UV optoelectronic applications over AlGaN. The third advantage is that with the correct choice of In and Al concentrations, lattice matching with GaN and energy gap engineering can be achieved during the growth of $In_xAl_yGa_{1-x-y}N$. A lattice-matched quaternary alloy is also seen to have better surface morphology. The limitation of critical thickness that is an issue in the growth of AlGaN due to lattice mismatch with GaN may not then be the case for $In_xAl_yGa_{1-x-y}N$. It is expected that detrimental effects due to lattice mismatch between the barrier and well materials, such as layer cracking, piezoelectric field, and high dislocation density will be significantly reduced in devices based on quaternary alloys compared with those

utilizing ternary alloys. This is very important for UV emitter and detector applications, where either AlGaN or InAlGaN will be used as active layers. Finally, the thermal coefficient of $In_xAl_yGa_{1-x-y}N$ is better matched to GaN than AlGaN is.

4. SUMMARY

In summary, $In_xAl_yGa_{1-x-y}N$ quaternary alloys have been grown by MOCVD on sapphire substrates. Optical properties of $In_xAl_yGa_{1-x-y}N$ quaternary alloys have been studied by picosecond time-resolved PL spectroscopy and compared with those of GaN epilayers as well as InGaN and AlGaN alloys. By controlling In and Al compositions of $In_xAl_yGa_{1-x-y}N$ quaternary alloys, we can achieve not only lattice match with GaN but also higher emission energies as well as higher emission efficiencies in the UV region in $In_xAl_yGa_{1-x-y}N$ quaternary alloys than that in GaN epilayers. In addition, PL emission intensity or quantum efficiency of $In_xAl_yGa_{1-x-y}N$ quaternary alloys is enhanced over $Al_xGa_{1-x}N$ alloys with similar Al contents and is comparable to that of $In_xGa_{1-x}N$ alloys with similar In composition. It is also demonstrated that the physical properties of $In_xAl_yGa_{1-x-y}N$ quaternary alloys are more closely related with $In_xGa_{1-x}N$ than $Al_xGa_{1-x}N$ including growth conditions and material properties. We have also fabricated ultraviolet (UV) photoconductive detectors based on $In_xAl_yGa_{1-x-y}N$/GaN quaternary alloy heterostructures. We found that with varying In and Al compositions, the cut-off wavelength of the $In_xAl_yGa_{1-x-y}N$ detectors could be varied to the deep UV range. The responsivity of the $In_xAl_yGa_{1-x-y}N$ quaternary alloys was found to exceed that of AlGaN alloys with comparable cut-off wavelengths by a factor of five. Just like the case in other conventional III-V semiconductor alloys, $In_xAl_yGa_{1-x-y}N$ quaternary alloys open a new avenue for the fabrication of many novel optoelectronic devices such as high efficient light emitters and detectors, particularly in the UV region. Additionally, the lattice matched $In_xAl_yGa_{1-x-y}N$/GaN ($y \sim 4.7\ x$) heterostructures also represent a unique system in which the piezoelectric field is absent and hence different effects of polarization and piezoelectric fields on the optoelectronic properties of III-nitride may be distinguished.

ACKNOWLEDGEMENTS

REFERENCES

E-mail: Jiang@phys.ksu.edu
1. S. Nakamura and G. Fasol, *The Blue Laser Diode*, Springer, New York, 1997.
2. R. A. Mair, J. Y. Lin, H. X. Jiang, E. D. Jones, A. A. Allerman, and S. R. Kurtz, Appl. Phys. Lett. **76**, 188 (2000).
3. J. Han, M. H. Crawford, R. J. Shul, J. J. Figiel, M. Bansa, L. Zhang, Y. K. Song, H. Zhou, and A. V. Nurmikko, Appl. Phys. Lett. **73**, 1688 (1998).
4. E. Munoz, E. Monroy, J.A.Garrido, I. Izpura, F.J. Sanchez, M.A. Sanchez-Garcia, E. Calleja, B. Beaumont, and P. Gibart, *Appl. Phys. Lett.* **71**, 870 (1997);
5. E. Monroy, E. Munoz, F.J. Sanchez, F. Calle, E. Calleja, B. Beaumont, P. Gibart, J.A. Munoz and F. Cusso, *Semicond. Sci. Technol.* **13**, 1042 (1998);
6. D. Walker, E. Munroy, P. Kung, M. Hamilton, F.J. Sanchez, J. Diaz and M. Razeghi, *Appl. Phys. Lett.* **74**, 762 (1999).
7. B.W. Lim, Q.C. Chen, J.Y. Yang, and M. Ashif Khan, *Appl. Phys. Lett.* **68**, 3761 (1996).
8. J.D. Brown, Z. Yu, J. Matthews, S. Harney, J. Boney, J.F. Schetzina, J.D. Benson, K.W. Dang, C. Terrill, T. Nohava, W. Yang and S. Krishnankutty, *MRS Internet J. Nitride Semicond. Res.* **4**, 9 (1999).
9. A. Osinsky, S. Gangopadhyay, B.W. Lim, M.Z. Anwar, M.A. Khan, D.V. Kuksenkov and H. Temkin, *Appl. Phys. Lett.* **72**, 742 (1998).
10. F. G. McIntosh, K. S. Boutros, J. C. Roberts, S. M. Bedair, E. L. Piner, and N. A. El-Masty, Appl. Phys. Lett. **68**, 40 (1996).
11. M. E. Aumer, S. F. LeBoeuf, F. G. McIntosh, and S. M. Bedair, Appl. Phys. Lett **75**, 3315 (1999).
12. S. F. LeBoeuf, M. E. Aumer, and S. M. Bedair, Appl. Phys. Lett. **77**, 97 (2000).
13. M. E. Aumer, S. F. LeBoeuf, S. M. Bedair, M. Smith, J. Y. Lin, and H. X. Jiang, Appl. Phys. Lett. **77**, 821 (2000).
14. M. Asif Khan, J. W. Yang, G. Simin, R. Gaska, M. S. Shur, and A. D. Bykhovski, Appl. Phys. Lett **75**, 2806 (1999).

15. M. Asif Khan, J. W. Yang, G. Simin, R. Gaska, M. S. Shur, Hans-Conrad zur Loye, G. Tamulaitis, A. Zukauskas, D. J. Smith, D. Chandrasekhar, and R. Bicknell-Tassius, Appl. Phys. Lett. **76**, 1161 (2000).

16 T. N. Oders, J. Li, J. Y. Lin, and H. X. Jiang, Appl. Phys. Lett. **77**, 791 (2000).

17. http://www.phys.ksu.edu/area/GaNgroup/

18. H. S. Kim, R. A. Mair, J. Li, J. Y. Lin, and H. X. Jiang, Appl. Phys. Lett. **76**, 1252 (2000).

19. L.S. Yu, D. Qiao, S.S. Lau, J.M. Redwing, J.Y. Lin and H.X. Jiang, *J. Appl. Phys.* **86**, 2696 (1999).

20. G. Parish, S. Keller, P. Kozodoy, J.P. Ibbetson, H. Marchand, P.T. Fini, S.B. Fleischer, S.P. DenBaars, U.K. Mishra and E.J. Tarsa, *Appl. Phys. Lett.* **75**, 247 (1999).